JOURNAL OF SOLID STATE CHEMISTRY 48, 100–116 (1983)

Defects in Hexagonal Vanadium Fluoride Bronzes: A High Resolution Electron Microscope Study

D. RIECK, R. LANGLEY,* AND L. EYRING†

Department of Chemistry and the Center for Solid State Science, Arizona State University, Tempe, Arizona 85287

Received September 1, 1982; in revised form February 2, 1983

Observations of hexagonal vanadium fluoride bronzes, A_xVF_3, (A = K, Rb, Cs, and Tl; $0.18 \leq x \leq 0.32$) by high resolution electron imaging showed the presence of several kinds of defects, including stacking faults, overlays, twin boundaries, and different types of antiphase boundaries. These defects were modeled, and the structures confirmed by comparison of calculated and observed images where necessary. The presence of disorder was interpreted as supporting evidence for the tentative phase diagram.

Introduction

Recently (*1, 2*) the structures of four phases present in the hexagonal vanadium fluoride bronzes, A_xVF_3, where A is K, Rb, Cs, or Tl and $0.18 \leq x \leq 0.32$ were described. These phases are superlattices of a hexagonal tungsten bronze (HTB) type unit cell. Samples were prepared (*3*) by firing stoichiometric amounts of VF_2, VF_3, and alkali metal fluoride, AF, in evacuated Mo capsules. Samples were annealed at 800°C for 30 days, then removed from the furnace to cool.

Table I lists the phases and the corresponding approximate unit cell dimensions. These dimensions vary with composition over a range of 0.12 Å for a and 0.15 Å for c. High A atom occupancy and/or a large A ionic radius favor larger lattice constants, but Vegaard's law is not followed. Phase α_I has the simplest structure. It contains a single hexagonal tunnel, and has a c axis the length of two VF_6 octahedra. The c axis diffraction pattern is a simple hexagonal array of spots separated by 0.16 $Å^{-1}$. Phase α_{II} is an orthorhombic superstructure of α_I containing four A atom sites in two hexagonal tunnels. The two tunnels have different A atom occupancy factors, not necessarily either integers or simple fractions. An $\alpha_{II}[001]$ diffraction pattern has superlattice spots halfway between each α_I spot in one a^* direction. The α_{III} phase has similar spots in an additional a^* direction. Phase α_{IV} is characterized by a c axis the length of six octahedra, three times that of the other phases. These superlattices are at least partially the result of ordering of A cations within and among the hexagonal tunnels. In this paper we discuss the defects observed in α_I and α_{II}, some of which also result from cation ordering. The phases α_{II}, α_{III}, and α_{IV} may also be considered as defect HTB

* Present Address: Department of Chemistry, Stephen F. Austin State University, Nacogdoches, Tex. 75961.

† Author to whom inquiries should be addressed.

0022-4596/83 $3.00

TABLE I

UNIT CELL PARAMETERS OF HEXAGONAL A_xVF_3 PHASES

	a	b	c	γ
α_I	7.39	7.39	7.53	120°
α_{II}	7.39	12.88	7.53	90°
α_{III}	14.78	12.88	7.53	90°
α_{IV}	7.39	*	22.59	*

* Undetermined, see text.

structures. Boo *et al.* (*3, 4*), also reported Jahn–Teller distortions of the structure of the sublattices from hexagonal symmetry.

The defects observed include twinning, stacking faults, coherent intergrowths, random filling of tunnels, overlays, and antiphase boundaries. Most of these defects were observed down the c axis. The twins, stacking faults, and overlays are only defined in α_{II}, since a 120° rotation of an α_I unit cell is trivial.

The electron diffraction patterns obtained from defects may be confused with those of another plane. This is especially true in X-ray powder diffraction of samples which are very large by TEM standards, but it is also true even of submicron size crystals in the electron microscope. The diffraction pattern of even a small selected area is subject to misinterpretation, since it may resemble that of a phase not actually present.

The mechanisms of cation ordering used to form pure phases are related to the formation of defects in these phases. Some defects which give information on cation ordering in the disorder-to-order transition (α_I to α_{II}) are discussed below. Also discussed are some defects which affect the sublattice.

Experimental Part

Samples of hexagonal vanadium fluoride bronzes with the general formula A_xVF_3 were supplied by W. O. J. Boo. The compositions examined in this study are listed in Table II. These samples span the entire range of x values for which the hexagonal tungsten bronze structure (or the related superstructure) is stable (*3*). Two to three hundred crystals were imaged at unit cell resolution, and diffraction patterns of several hundred other crystals were obtained. The samples $K_{0.225}VF_3$ and to a lesser extent $K_{0.25}VF_3$, $Rb_{0.25}VF_3$, and $Rb_{0.32}VF_3$ were studied much more extensively than the others, partly because defects were more numerous in these samples. Sample preparation and examination were as described previously (*1*). The images and diffraction patterns were taken on a JEOL JEM-100B transmission electron microscope. While the occasional crystals of VF_3 which were seen decomposed immediately in the electron beam, the hexagonal bronze samples were stable indefinitely under normal imaging conditions. As reported in (*1*), electron beam heating could induce limited, local movement of potassium ions in tunnels but the VF_6 octahedra were not damaged.

Results and Discussion

a. Axis Doubling

Two types of ordering can mimic the $[001]\alpha_{III}$ diffraction pattern. The first type is a [110] twin (Fig. 1) resulting from two areas of α_{II} coming together at 120°. In the different twin orientations a different one of

TABLE II

SAMPLES OF HEXAGONAL VANADIUM FLUORIDE BRONZES (A_xVF_3) INVESTIGATED

A	x				
K	0.18	0.225	0.25	0.27	
Rb	0.18	0.225	0.25		0.32
Cs	0.18		0.25		0.32
Tl	0.18		0.25		0.33

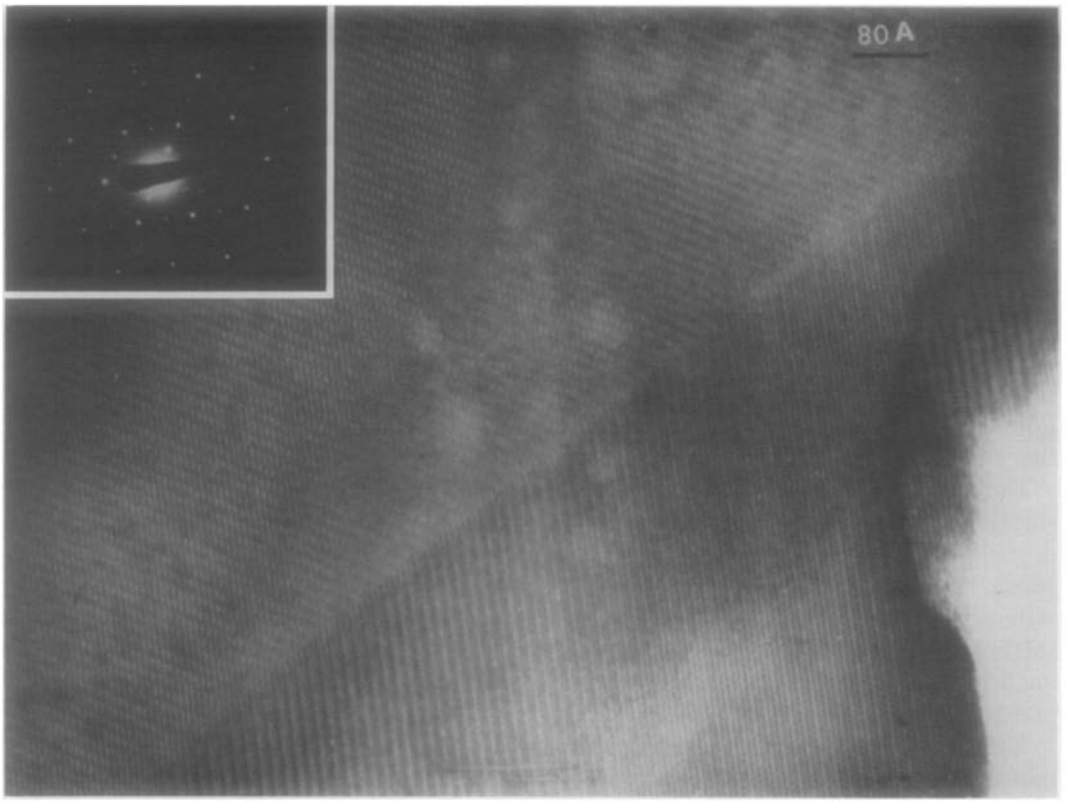

FIG. 1. Twinning in a phase α_{II} sample of $Tl_{0.18}VF_3$.

the hexagonal a axes is doubled. The VF_3 sublattice remains essentially unchanged, with the twin resulting only from ordering of the Tl cations. The result is that the fringes showing the alternating arrangement of dark and light rows of tunnels (doubled a axis) are seen to be rotated by 60°. Evidence for a small number of other isolated twin boundaries in thick crystals exists, but is not confirmed. No images suggest multiple or ordered twinning.

The electron diffraction pattern of an area including the twin boundary would be expected to resemble that of α_{III} (*1*). The twin orientations would each produce a set of superstructure spots which together would produce a pattern that could be interpreted as containing a hexagonal tungsten bronze structure with two doubled a axes. If equal areas of each orientation were present in the diffraction aperture the two sets of superlattice spots would be of equal intensity, as proposed for α_{III}. However, the diffraction pattern is strongly noncentrosymmetric, and thus easily distinguished from α_{III}. The rare case of equal twin areas or several closely spaced twin boundaries, or twinning at the unit cell level, could result in an α_{III}-type diffraction pattern, but there is no evidence from the images that any of the samples contained such defects.

A similar diffraction pattern would result from having an area of α_{II} covered by another area in which the cations were ordered so as to double a different a axis. Such overlays are discussed later, along with the related Moiré fringes which sometimes accompany them.

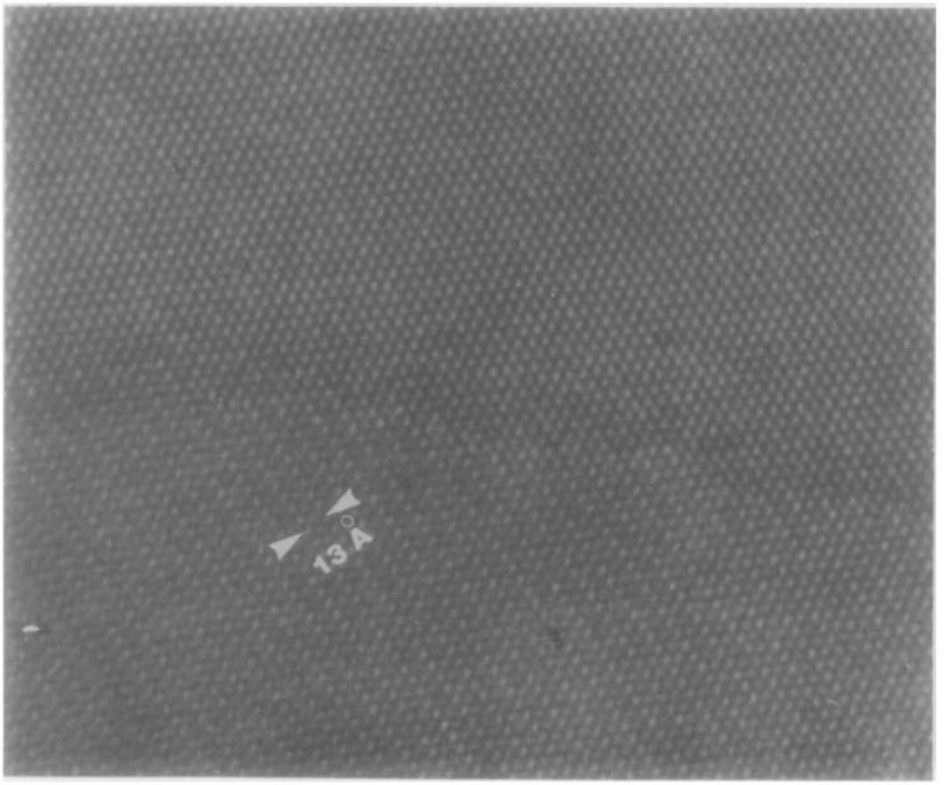

FIG. 2. Coherent intergrowth of phases α_I and α_{II} in a $Tl_{0.33}VF_3$ crystal viewed down [001].

In X-ray powder patterns (*3*), the presence of α_I in a sample containing α_{II} could only be discerned by careful quantitative measurement of intensities. Figure 2 shows that these two phases do intergrow coherently, making it difficult to separate two areas of a crystal even in a microscope by diffraction alone. High-resolution imaging confirms unambiguously the presence of α_I.

Coherent intergrowth of phases α_I and α_{II} as shown in Fig. 2 has been observed occasionally. One problem in interpreting coherent intergrowths is that for very thin regions (less than 30 Å) calculated images indicate that it can be difficult to distinguish α_I from α_{II}. Therefore, what appears to be a coherent intergrowth may only be a thickness effect. Because of this complication α_I–α_{II} boundaries were assumed to be coherent intergrowths only in thicker regions of crystals. Calculated images indicate that the region in Fig. 2 is greater than 60 Å thick; therefore the boundary is not an artifact of the thickness.

Uneven contrast suggests that in some crystals, especially in very thin regions, the filling of the tunnels by *A* ions is irregular (see Fig. 3). This irregular filling was observed in about a quarter of the very thin crystals of Rb_xVF_3, and occasionally in samples containing Cs and Tl. The degree of variation is uncertain for the same reasons that it is impossible to determine the absolute filling of the tunnels in the ordered regions (*1*). These defects appear to be random since they are not observed in thicker regions where the effect would be averaged out. These could be considered point de-

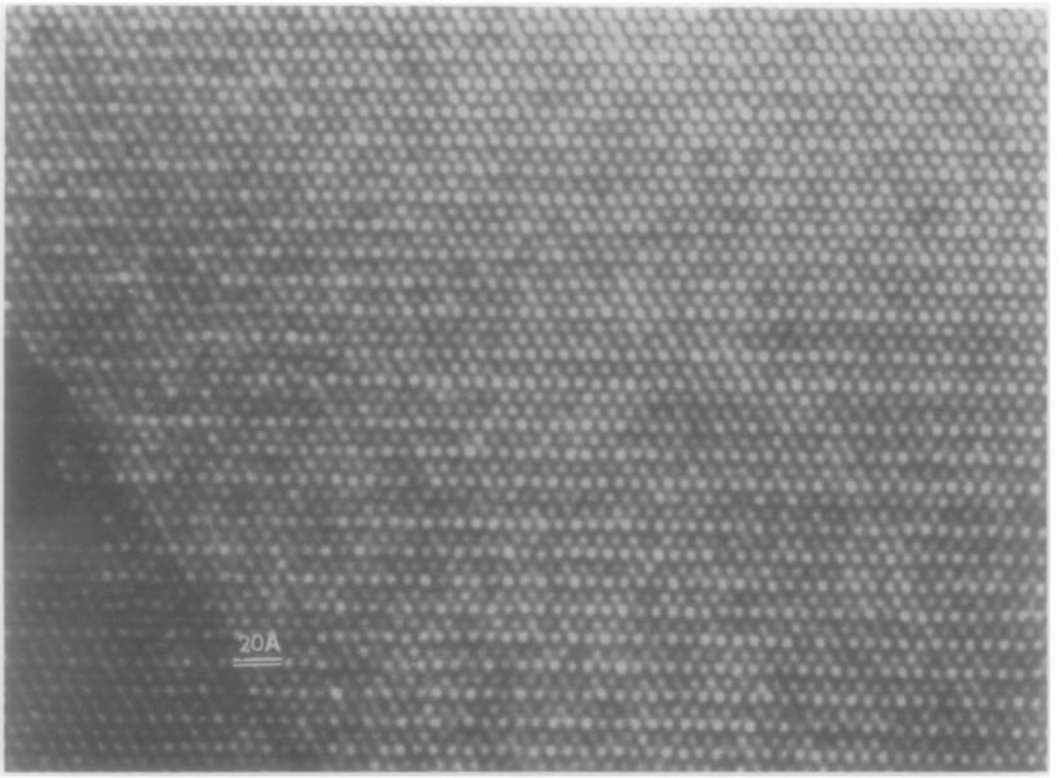

FIG. 3. Images of $Rb_{0.32}VF_3$ showing randomly spaced projections of tunnels of different brightness (filling).

fects since in the thin regions where they are observed there are so few lattice sites available for the *A* ions that a variation of more than an atom or two is not possible.

Stacking Faults

If the transition from α_I to α_{II} were complete, and the products had reached equilibrium, the distribution of defects observed in the microscope in a given sample would be essentially invariant. This is not the case. If, as believed (*1*), α_I and α_{II} are separated by temperature rather than composition, the presence of α_I in the sample at room temperature also indicates that the reaction did not go to completion. The presence of α_I and α_{II} together and the variable distribution of defects in α_{II} thus support the same conclusion.

The density of defects was particularly high and uneven in α_{II}-$Rb_{0.32}VF_3$ samples. This is assumed to be because the large size of the rubidium atom would make the ordering transition more difficult than for potassium. Crystals containing the very large cesium atoms remained α_I on cooling. The large number of defects in $Rb_{0.32}VF_3$ may also indicate instability of α_{II} at that composition.

Differences in ordering between regions are indicated by overlays, twin boundaries, and phase boundaries. Disorder on a unit cell level is shown by stacking faults and point defects. Stacking faults were commonly observed in regions of α_{II} as shown in Fig. 4. Such faulting produces streaking in the electron diffraction pattern. Irregular ordering of the cations is probably the

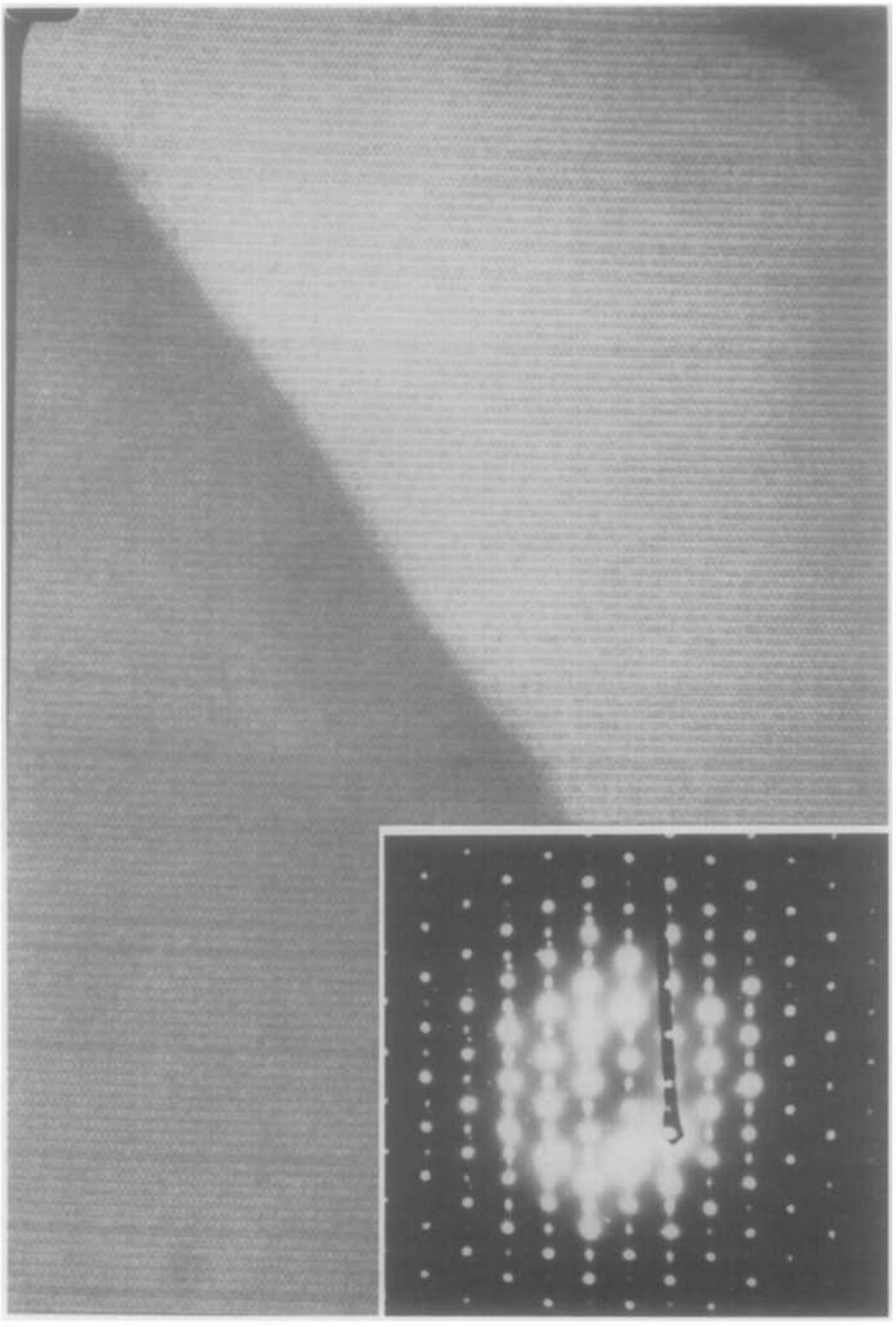

FIG. 4. An image showing stacking faults in phase α_{II} $Rb_{0.32}VF_3$. Note the streaking in the inserted diffraction pattern.

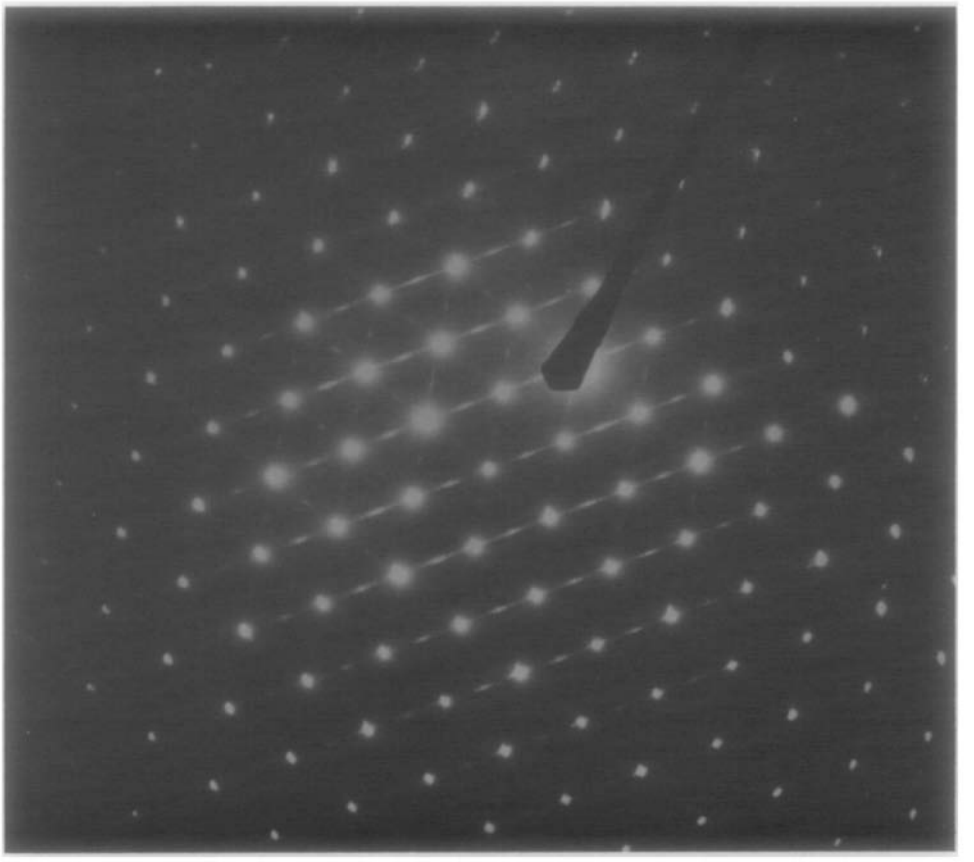

FIG. 5. An electron diffraction pattern thought to be due to stacking faults in three orientations. An image of this crystal ($Rb_{0.32}VF_3$) was not obtained because it was too thick.

cause of such defects. Streaking in two or three directions in the diffraction pattern was also observed (see Fig. 5). Good images for crystals exhibiting multidirectional streaking were not obtained because the crystals were too thick. It is possible that in any one crystallographic plane faulting in more than one direction may be inhibited and it is only in thicker crystals that enough planes containing faults in different directions are present.

Since the projection of the potential is the most important factor in determining the image, an area containing a twin boundary in α_{II} may have an image very similar to an area where part of the crystal is covered with a layer of α_{II} in which a different a axis is doubled. Figure 6 shows an image where an area of α_{II} overlays another area of α_{II}, the b axis of which is rotated 60° from that of the first. The overlap of the two directions of the fringes is most clearly seen just above the shadow of the beam stop.

A phenomenon that is possibly related to stacking faults is indicated by the presence of Moiré fringes. These fringes result from slight differences in layers perpendicular to the electron beam. These differences must produce a slightly misaligned structure. Figure 7 shows an example of a region containing several Moiré fringes. At least 10 such regions were imaged in potassium

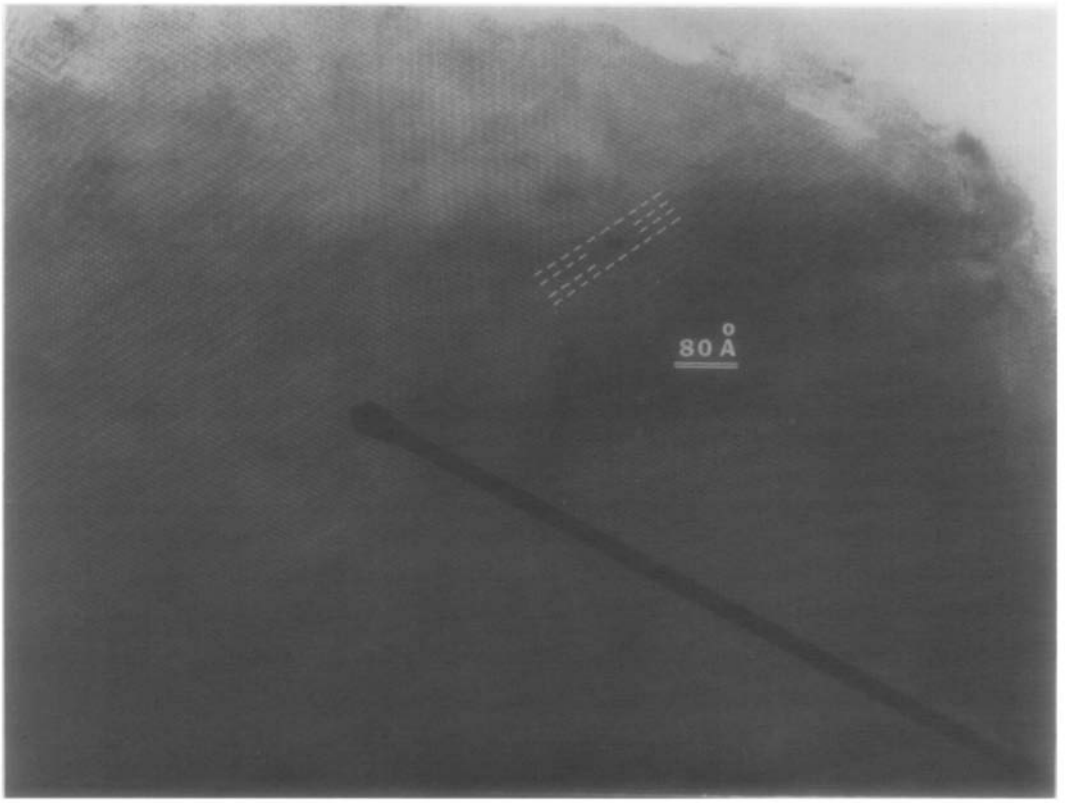

FIG. 6. Overlay (or twinning) in $K_{0.225}VF_3$. In the lower part, the α_{II} fringes are in register across the vertical band. The fringes are displaced by half of a unit cell in the upper part by the edge dislocation outlined.

containing samples. The differences in the layers in the bronzes could be caused by several types of defects or by a combination of defects. For example, compositional variations can occur which result in slight alterations of the lattice to accommodate the different numbers of *A* ions. Jahn–Teller distortion (*3, 4*) also increases with increasing *A* ion content, due to the reduction of V^{III} to V^{II}. It is also possible that part of the crystal is one phase (i.e., α_I) and part is another (i.e., α_{II}). This would also give rise to a slight lattice distortion, especially if α_I were only pseudo-hexagonal (monoclinic). The discussion of "distortion ratios" (*3*) considers only α_{II}, but lends support to a lower symmetry for α_I.

Another possibility is that in α_{II}, doubling may occur along different *a* axes in different layers, and since the doubling of *a* is not exact, the alignment of the different layers will not be exact. Doubling of more than one *a* axis as well as some of the other features described here have been observed within one layer. An extreme example of doubling of different *a* axes in different layers is to have each of the three *a* axes doubled. Such an arrangement could give rise to a hexagonal Moiré pattern like the one shown in Fig. 8. Change in occupancy or inclusion of α_I would result in no noticeable difference in the diffraction pattern, while the third case would produce a diffraction pattern similar to that for a twinned region,

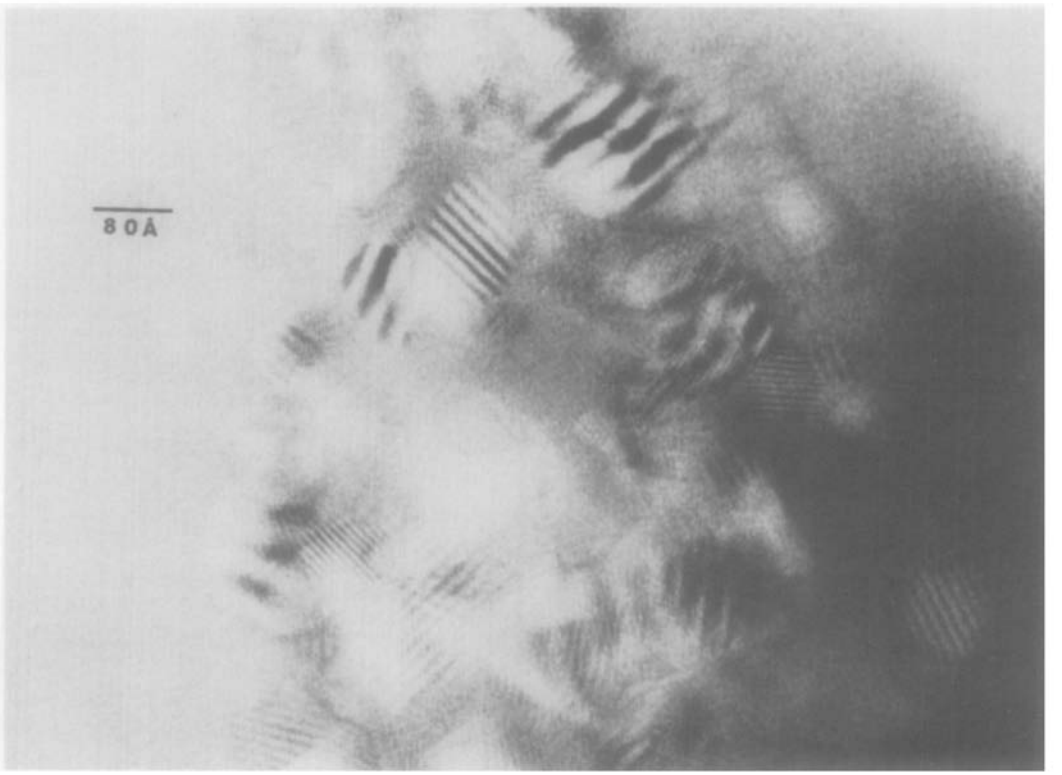

FIG. 7. Moiré fringes observed in $K_{0.25}VF_3$.

but with three sets of superlattice spots. Several such diffraction patterns were observed.

Sublattice Defects

Figure 9 shows an image from $K_{0.25}VF_3$ containing several defects. The inset diffraction pattern was taken with a field-limiting aperture centered on the defect in the center of the figure. The area contributing to the diffraction pattern corresponds to a circle with its center near the bottom of the figure, and tangent to the top.

The material on the left is clearly shown, by the hexagonal diffraction pattern and the image details, to be a c axis projection. The essential features of the defects present in the left side are that they are coherently intergrown with the hexagonal lattice, and that a displacement of the lattice vectors by $a/2$ takes place when the defect is crossed. These considerations give rise to the model shown in Fig. 10. The atom positions drawn are idealized and approximate. The fluorine atoms lying directly in the defect plane are expected to be displaced in a zig-zag fashion from the positions shown, but this cannot be experimentally verified. Overall, the distortion present in the VF_6 octahedra is not unacceptably large.

The defect is a translational antiphase boundary which can formally be described as a slip, or a translation of one side of the lattice by $a/2$ with respect to the other. These defects are assumed to have grown in the lattice, rather than to have been induced. The growth mechanism may have initially involved substitution of vanadium

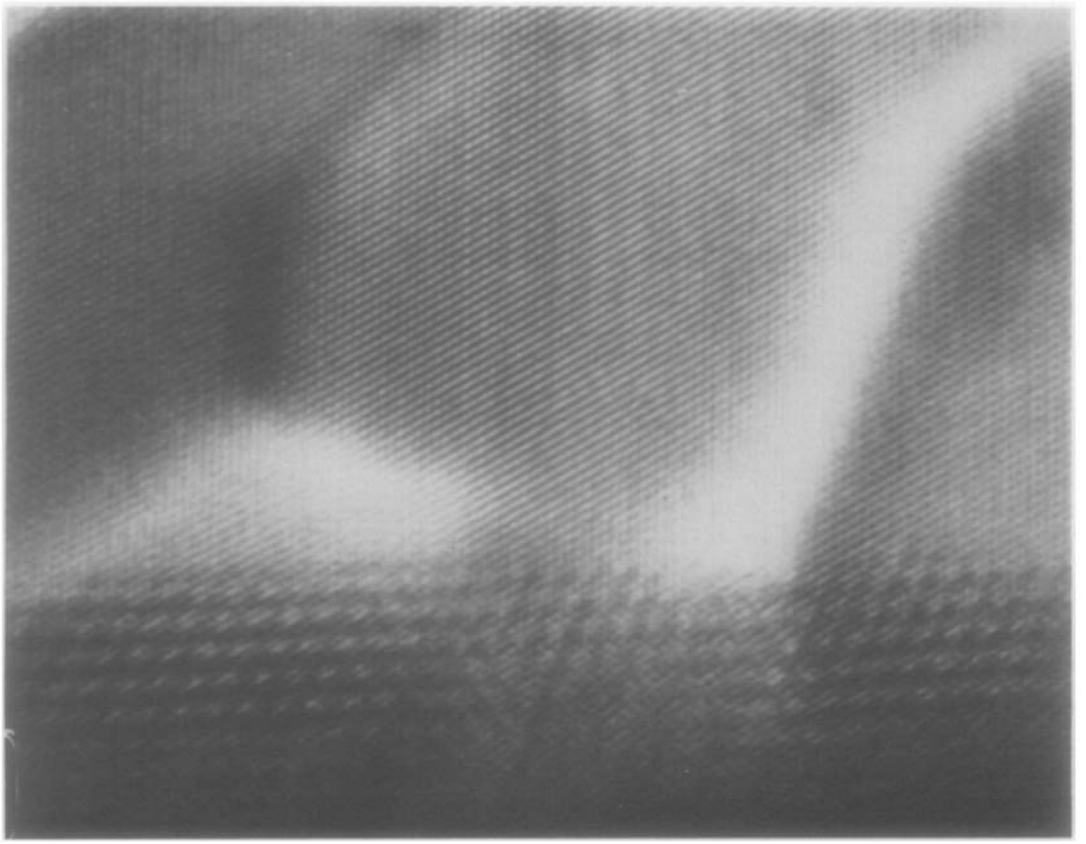

FIG. 8. Moiré fringes in $Rb_{0.32}VF_3$ indicating misalignment of all hexagonal *a* axes. The repeat distance between Moiré spots is 24.4 Å.

in potassium positions, and vice versa, with the fluoride ions adjusting accordingly.

A comparison between the image of the defect and an image calculated using the atom positions shown in Fig. 10 as a model is shown in Fig. 11. Although the tunnels do not appear to be directly across from each other in the image of the thicker part of the crystal, the match is good at the top of the inset. The defocus value at the top of the inset is apparently near optimum, and the thickness at that point was determined by comparing the oscillation of the calculated transmitted intensity for the central beam vs sample thickness (Fig. 12) with the extinction contours in Figs. 9 and 11. The contrast in Fig. 9 has been selectively lightened in the printing of the photograph. This makes the extinction contours less well defined, but the overall image much clearer. The image contrast in Fig. 11 is a true representation.

The interpretation of the defect down the middle of Fig. 9 is a more difficult problem. Careful measurement of enlargements of this boundary indicate that the intergrowth is coherent, but the diffraction pattern and iamge both show that the right side has orthorhombic symmetry, rather than hexagonal.

Referring again to Fig. 10, it is seen that four potassium positions paired across the

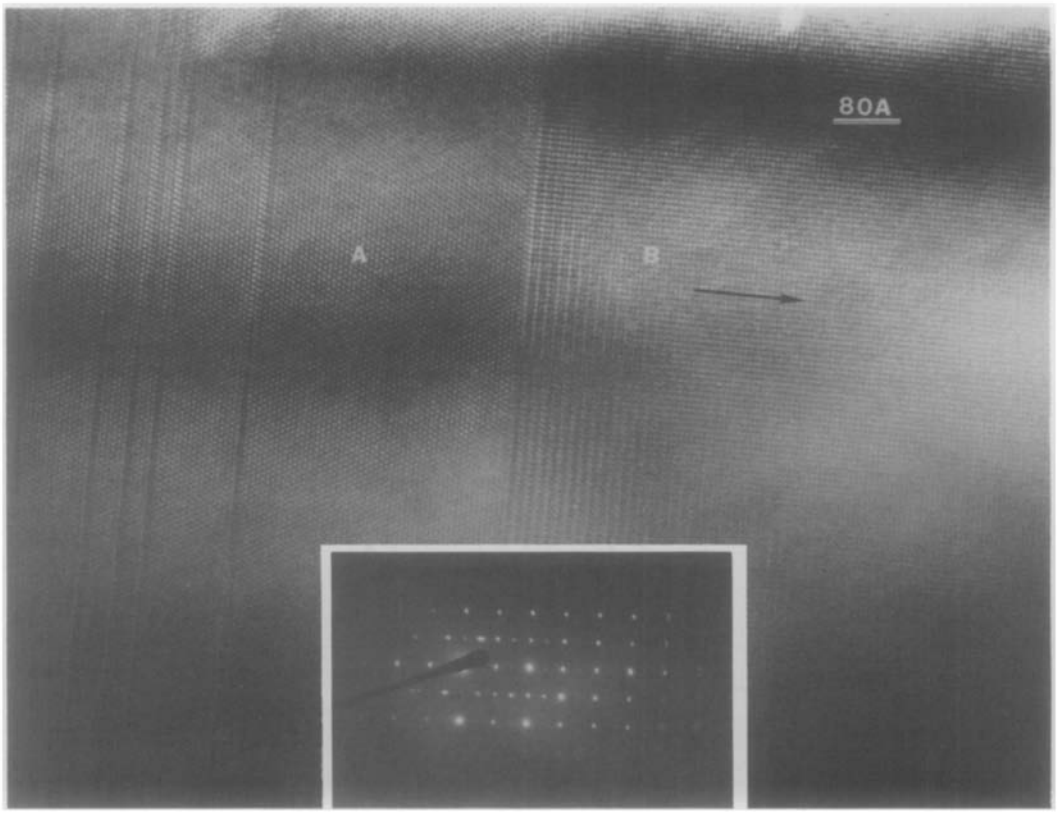

FIG. 9. An image from $K_{0.25}VF_3$, with an inset diffraction pattern from a small area. The area labeled A is projected in [001], the B area is projected in [100]. The arrow is parallel to [120].

boundary can be used to define an orthohombic unit cell. This unit cell has the same composition and volume as the hexagonal HTB type cell of the surrounding crystal. It is tempting to assume on this basis that the right side of Fig. 9 is a polymorph of hexagonal $K_{0.25}VF_3$, having this unit cell derived from the nearby translational boundaries. A variety of evidence suggests a different conclusion, however.

A series of images calculated assuming an infinite lattice composed of polymorph cells is shown on the left in Fig. 12. The agreement between these images and the enlarged experimental image (from a different plate than Fig. 9) is not satisfactory for any set of imaging parameters. Calculations and comparison with hexagonal $K_{0.25}VF_3$ from the [100] direction (right side of Fig. 12) show very good agreement, however. The main difference between the projected potential in $[100]_{hex}$ and $[001]_{poly}$ is that for the $[100]_{hex}$ projection, there are streaks approximately every 3.7 Å, due to the alternation of relatively dense layers of composition VF_2 with layers of KF or $K_{0.5}F$. For the *c* axis projection of the polymorphic cell, the streaks are separated by the longest distance between potassium sites, which is 7.39 Å. In a thin crystal, the wide, dark band in the image is due to the VF_2 lattice, while the lighter streak results from the

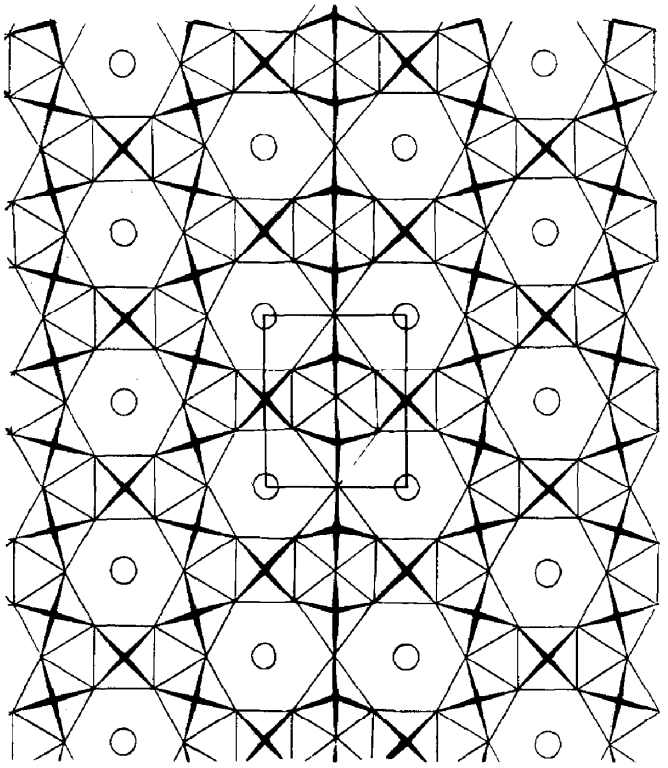

FIG. 10. A line drawing of a model of the translational antiphase boundary on the left side of Fig. 9.

lower potential of $K_{0.75}F$ along the direction in which the K sites are separated only by single fluoride ions. There is no structural feature which would produce a periodicity of one half of 7.39 Å.

Another important evidence is the superlattice spots in the diffraction pattern indicating a tripling of the lattice parameter in the vertical direction. These show much more clearly on the original plate than on the Fig. 10 inset. These spots show the existence of the α_{IV} phase within the field-limiting aperture. Phase α_{IV} is seen in images of the lower right part of this crystal, outside the area included in Fig. 9. The axis that is tripled in α_{IV} is c (*4*), and therefore the line on which these superlattice spots lie must be c^* of the hexagonal structure. The c axis is therefore vertical on the right side of Fig. 9. The black arrow on the right side indicates the [120] direction. It is interesting that this is parallel to the [120] direction on the left side. The boundary can thus be described as a rotation of the structure by 90° about the $[120]_{axis}$, and is named a rotational antiphase boundary. It might also be called an "*ac*" or "[100][001]" boundary, according to the axes which are parallel in this projection. A model of this has been built, and is shown in Fig. 13. Compare the model with the top center of Fig. 9.

If viewed from a direction 90° to the image axis of Fig. 9, in the plane of the boundary, the boundary should appear identical except that the hexagonal pattern would be on the right side and the orthohombic on the left. The two sides of such a boundary are therefore equivalent, and cannot be distinguished in an absolute way. Such boundaries should resist annealing indefinitely,

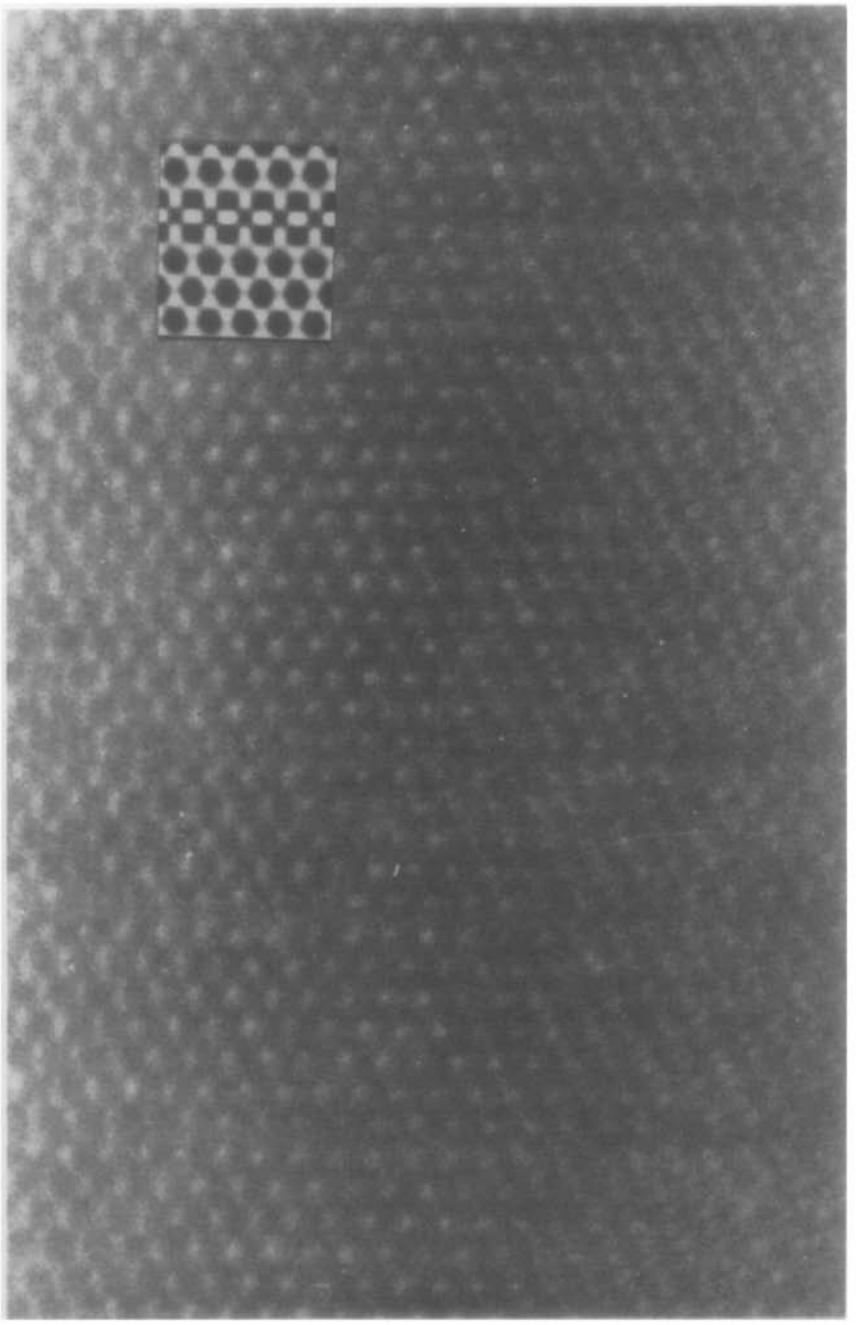

FIG. 11. An enlargement of translation boundaries with calculated image based on Fig. 10 as inset. The four boundaries are readily apparent if the figure is viewed on edge.

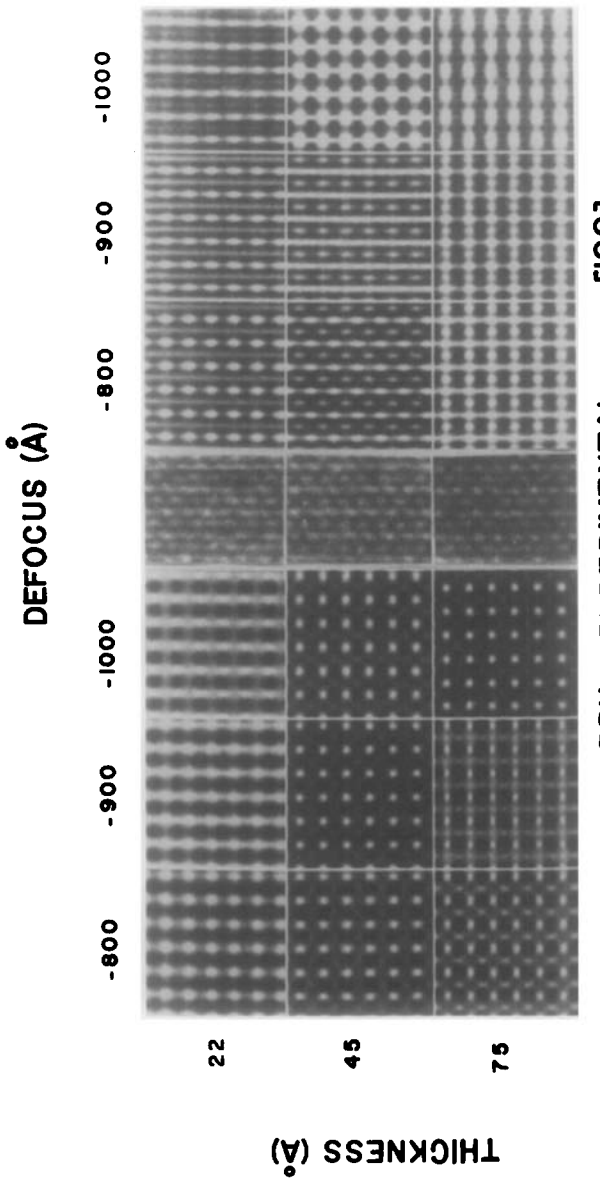

FIG. 12. Comparison of the experimental image with images calculated for α_I $K_{0.25}VF_3$, [100] projection, and for a $K_{0.25}VF_3$ polymorph of α_I.

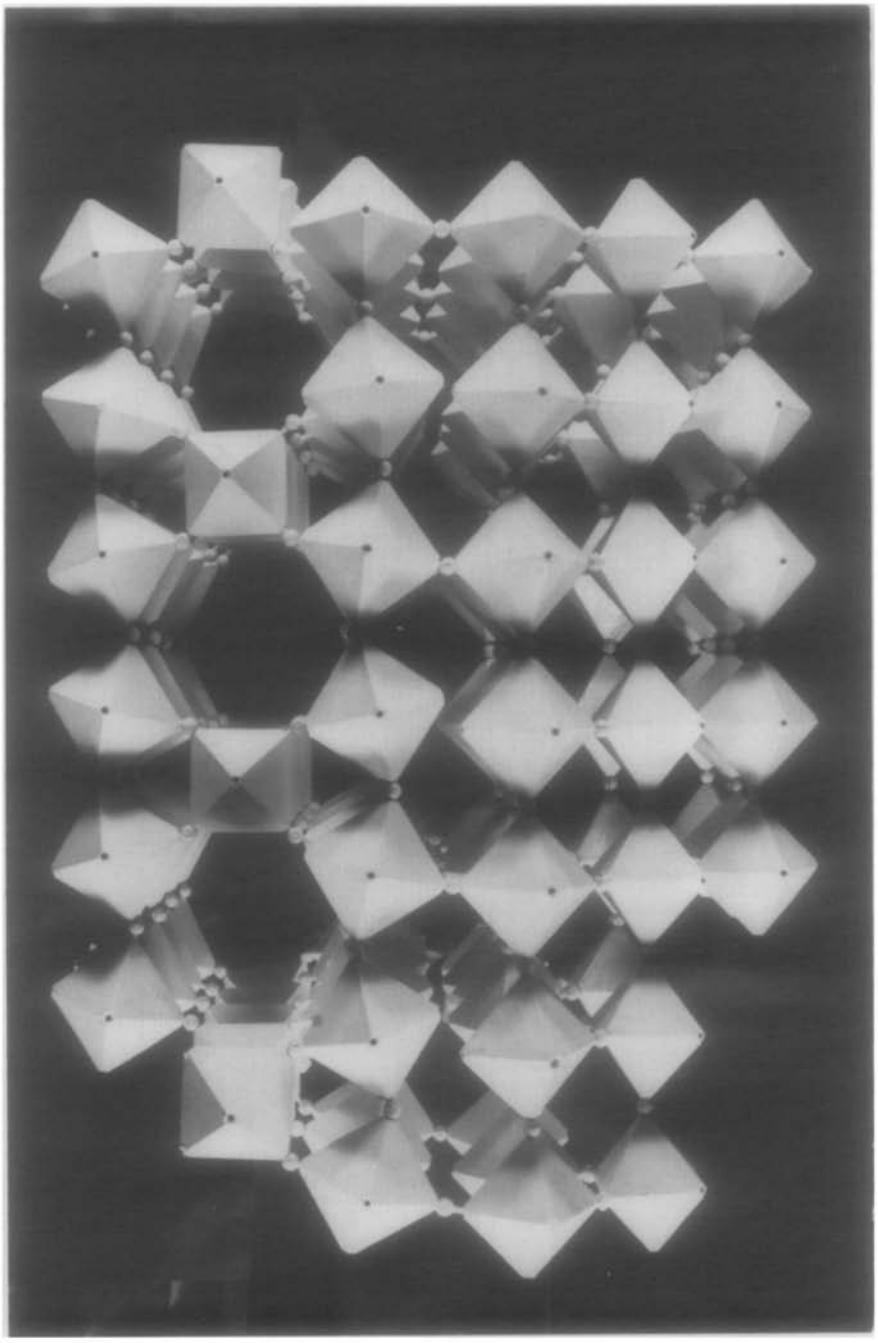

FIG. 13. Model of the *ac* boundary, illustrating coherent intergrowth over a length of 23 Å.

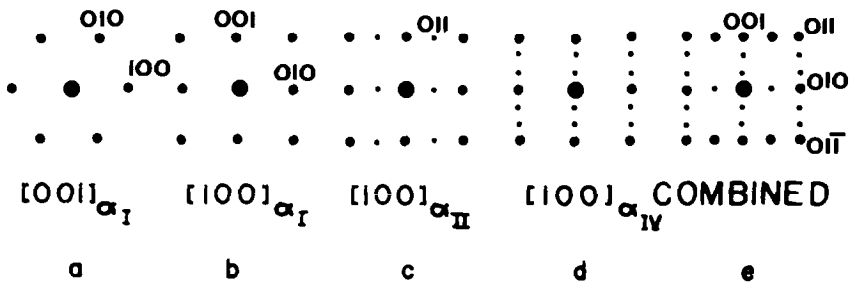

FIG. 14. Diffraction patterns from the hexagonal bronze structure. (a) [001] projection of α_I, (b) [100] projection of α_I, (c) [100] projection of α_{II}, (d) [100] projection of α_{IV}. (Note superstructure spots of (c) and (d).) (e) Superposition of all four patterns. Notice that the $[100]_{\alpha_{II}}$ superlattice spots are eclipsed by the $[001]_{\alpha_I}$ spots on odd layer lines only.

since there is no preferred direction of movement. Note also that translational boundaries like those on the left side may be present on the right, but not visible except for a possible strain field, since the lattice translation would be parallel to the image axis.

The inset to Fig. 9 is actually an overlap of four different diffraction patterns. Figure 14,a–d shows the four separate patterns, drawn to the same scale, with appropriate identification. The major spots are the same for Fig. 14,b, c, and d. Overlap of spots from 14,a with those of the other patterns is possible because the *a* and *c* axes are nearly the same length, or even fully the same length (see below). When the first four patterns are superimposed, they result in e, which is like the Fig. 9 inset. It is convenient to index e the same as b. Along the $0k0$ layer line of e (horizontal), the spots from the $[100]_{\alpha_I}$ and $[001]_{\alpha_I}$ projections overlap. On the $0k1$ and $0k\bar{1}$ layer lines, $hk0$ (k odd) spots from $[001]_{\alpha_I}$ appear in the position of α_{II} superlattice spots (011) in $[100]_{\alpha_I}$. On the α_{IV} superlattice, spots are most visible between $[03\bar{1}]$ and $[03\bar{2}]$ (positive b^* is to the right, c^* is up). These spots are clearly visible between several pairs of spots in that quarter of the pattern on the original plate.

This *ac* model of the boundary does not account for the apparent coherence. Although Fig. 14 clearly demonstrates the plausibility of the model, in that the strain is low enough that it can be built with rigid octahedra over a length of three unit cells, it is not actually coherent. The left side of the boundary has a periodicity of 7.39 Å, while the right side has a periodicity of 7.53 Å, which are the *a* and *c* axis lengths, respectively. The difference between them is one part in 53, so every 53 unit cell lengths (400 Å) there should be a discontinuity. The boundary is visible for nearly 200 unit cell lengths on the original plate, and careful measurement of enlarged prints does not reveal any mismatch.

Boo (*3*) describes distortion of the lattice from true hexagonal symmetry. The distortion necessary to bring the *a* axis length up to 7.53 Å is not far outside the limit of error given in his paper for the distorted *a* lattice parameter. An increase in the acute angle from 60 to 61.3° would lengthen one *a* axis to 7.53 Å, and thus allow the boundary to be coherent. The fact that identical adjustments must be made in two directions does not necessarily complicate the problem. Translational antiphase boundaries are observed in three other cases, and rotational boundaries in two. One rotational boundary was curved (80° of arc in 1000 Å) and the other was also in proximity to translational boundaries. This suggests that there is doubtless some correlation between the presence of the translational boundaries

and this rotational boundary—perhaps related to the strain. Although the polymorph model of the lattice accounts fully for the coherent intergrowth, the evidence of the calculated images, and particularly the presence of α_{IV}, outweighs support for the polymorph model.

Acknowledgments

The authors gratefully acknowledge support by the National Science Foundation through Grants DMR 8006584 and DMR 8108306 for research, and through Grant CHE 7916098 which supports the Regional Instrumentation Center for High Resolution Electron Microscopy. The authors also would like to thank Dr. A. R. Rae-Smith for reading the rough draft and making useful suggestions.

References

1. D. Rieck, R. Langley, and L. Eyring, *J. Solid State Chem.* **45,** 259 (1982).
2. R. Langley, D. Rieck, H. Eick, L. Eyring, R. F. Williamson, and W. O. J. Boo, *Mater. Res. Bull.* **13,** 1297 (1978).
3. Y. S. Hong, R. F. Williamson, and W. O. J. Boo, *Inorg. Chem.* **18,** 2123 (1979).
4. Y. S. Hong, R. F. Williamson, and W. O. J. Boo, *Inorg. Chem.* **20,** 403 (1981).